2013 European Control Conference (ECC)
July 17-19, 2013, Zürich, Switzerland.

Feedback Perimeter Control for Multi-region Large-scale Congested Networks

Konstantinos Aboudolas and Nikolas Geroliminis

Abstract— **It was recently observed from empirical traffic data that by aggregating the highly scattered plots of flow versus density from individual loop detectors for city regions with homogeneous spatial distribution of congestion, the scatter significantly decreases and a well-defined Macroscopic Fundamental Diagram (MFD) exists between space-mean flow and density. This result can be of great importance to unveil simple perimeter control policies in such a way that maximizes the network outflow (trip endings). Single-region perimeter control might be sub-optimal if there is a significant number of destinations outside the region of analysis or if the network is heterogeneously loaded. This paper integrates an MFD modeling to perimeter and boundary control optimization for large-scale networks with multiple centers of congestion, if these networks can be partitioned into a small number of homogeneous regions. Perimeter control actions may be computed in real-time through a linear multivariable feedback regulator. The impact of the perimeter control actions to a three-region real urban network is demonstrated via micro-simulation. A key advantage of the proposed approach is that it does not require high computational effort and future demand data if the current state of each region can be observed.**

I. Introduction

One of the most broadly used laws in traffic flow theory is the *Fundamental Diagram* (FD) which was initially observed for a stretch of highway [1] provides a steady-state relationship between traffic variables (speed, density, and flow). Although quite capable in providing a coarse description of main traffic features (e.g. formation and dissolution of shockwaves), the FD is inadequate in describing some complex traffic patterns such as stop-and-go waves, capacity drop phenomena, etc. (see [2], [3]). Recently, however, it was observed from empirical data in Yokohama, Japan [4] that by aggregating the highly scattered plots of flow versus density from individual loop detectors, the scatter almost disappeared and a well-defined diagram exists between space-mean flow and density. This field experiment showed that if congestion is homogeneously distributed (i) urban neighborhoods approximately exhibit a *Macroscopic Fundamental Diagram* (MFD) relating the number of vehicles to space-mean speed (or flow), (ii) there is a robust linear relation between the neighborhood's average flow and its outflow, and (iii) the MFD is a property of the network infrastructure and control and not of the demand. Other empirical and simulation studies for MFDs can be found in [5], [6], [7], [8]. Despite the recent findings for well-defined MFDs with low scatter in homogeneous networks, in reality many networks are heterogeneous with different congestion conditions and these curves should not be a universal law. For example, recent simulation and empirical findings [9], [10], [3] have shown that hysteresis phenomena exist in MFDs for urban and freeway networks.

One can model a network as single or multi-reservoir system (see Figs 1(a) and 1(b), respectively) depending on the geometry and the spatial distribution of congestion in the network. Networks with an uneven distribution of congestion may exhibit traffic states that are too scattered to line along an MFD and require partitioning [11]. These findings are of great importance because the concept of an MFD with optimum accumulation can be applied for heterogeneous networks with multiple centers of congestion and unveil simple perimeter control policies in such a way that maximizes the network capacity and outflow. The general idea of a *perimeter control policy* is to *meter* the input flow to the system and to hold vehicles outside the system if necessary [12]. Recently, this simple idea has been an issue of investigations for single-region [13] and two-region systems [14]. Single-region perimeter control [12], [13] might be suboptimal if there is a significant number of destinations outside the region of analysis. Moreover, single-region perimeter control may induce uneven distribution of vehicles in the reservoirs, and, as a consequence, may invalidate the homogeneity assumption of traffic loads within the reservoirs and degrade the network throughput. It might not be equitable as well given that all the penalties of waiting are transferred to external vehicles moving from outside to the study region. On the other hand, the authors in [14] developed a Model Predictive perimeter Control (MPC) strategy for a hypothetical closed-loop network with two regions. However, MPC requires that future demands be predicted, and thus more effort is needed for online use.

In this paper, a generic mathematical model of an N-reservoir network with well-defined MFDs for each reservoir is presented first. Then, an optimal control methodology is employed for the design of perimeter control strategies that aim at distributing the accumulation in each reservoir as homogeneously as possible, and maintaining the rate of vehicles that are allowed to enter each reservoir around a desired point, while the system's throughput is maximized. Based on this control methodology, perimeter control actions may be computed in real-time through a linear multivariable feedback regulator (LQ). To this end, the heterogeneous network of the Downtown of San Francisco is partitioned into three homogeneous regions that exhibit well-defined MFDs (according to [11]). These MFDs are then used to design the

K. Aboudolas and N. Geroliminis are with the Urban Transport Systems Laboratory, School of Architecture, Civil & Environmental Engineering, École Polytechnique Fédérale de Lausanne, CH-1015 Lausanne, Switzerland E-mail: konstantinos.ampountolas@epfl.ch, nikolas.geroliminis@epfl.ch

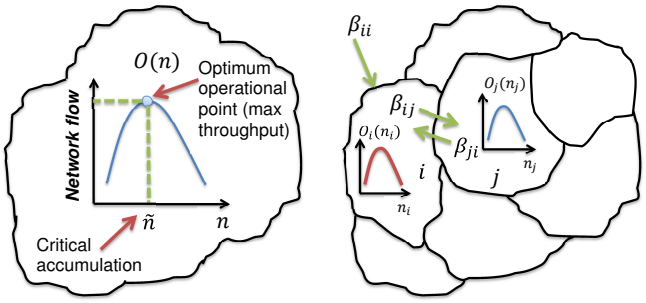

(a) (b)

Fig. 1. A network modeled as (a) single or (b) multi-reservoir system.

LQ regulator. Finally, the impact of the perimeter control actions to the three reservoirs and the whole network is demonstrated via simulation by the use of the corresponding MFDs and other performance measures.

II. Dynamics for Large-Scale Networks Partitioned in N Reservoirs

Consider a network partitioned in N reservoirs (Fig. 1(b)). Denote by $i = 1, \dots, N$ a reservoir in the system, and let $n_i(t)$ be the accumulation of vehicles in reservoir i at time t; $n_{i,\max}$ be the maximum accumulation of vehicles in reservoir i. We assume that for each reservoir $i = 1, \dots, N$ there exists an MFD, $O_i(n_i(t))$, between accumulation n_i and output O_i (number of trips exiting reservoir i per unit time either because they finished their trip or because they move to another reservoir), which describes the behavior of the system when it evolves slowly with time t.

Let $q_{i,\text{in}}(t)$ and $q_{i,\text{out}}(t)$ be the inflow and outflow in reservoir i at time t, respectively; $\mathcal{S}_i$ be the set of origin reservoirs which are reachable from reservoir i. Also, let $d_i(t)$ be the uncontrolled traffic demand (disturbances) in reservoir i at time t. Note that $d_i(t)$ includes both internal (off-street parking for taxis and pockets for private vehicles) and external (non-controlled) inflows. The conservation equation for each reservoir $i = 1, \dots, N$ reads

$$\frac{dn_i(t)}{dt} = q_{i,\text{in}}(t) - q_{i,\text{out}}(t) + d_i(t). \tag{1}$$

Since the system of each reservoir evolves slowly with time, we may assume that the outflow $q_{i,\text{out}}(t)$ is function of the output $O_i(n_i(t))$ (the MFD), where output $O_i(n_i(t))$ is the sum of the exit flows from reservoir i to reservoir j, plus the internal output (internal trip completion rates at i). If i and j are two reservoirs sharing a common boundary, we denote by β_{ji} ($j \neq i$) the fraction of the flow rate in reservoir j that allowed to enter reservoir i and by β_{ii} the fraction of the flow rate in the perimeter of the network allowed to enter reservoir i (see Fig. 1(b)). The inflow to reservoir i is given by

$$q_{i,\text{in}}(t) = \sum_{j \in \mathcal{S}_i} \beta_{ji}(t - \tau_{ji}) O_j(n_j(t)) \tag{2}$$

where $\beta_{ji}(t - \tau_{ji})$ are the input variables from reservoir j to reservoir i at time t, to be calculated by the perimeter controller, and τ_{ji} is the travel time needed for vehicles to approach reservoir i from the origin reservoir j. Without loss of generality, we assume that $\tau_{ji} = 0$, i.e., vehicles can immediately get access to the reservoirs of the network. This assumption can be readily removed by introducing additional auxiliary variables. Additionally, $\beta_{ji}(t)$ is constrained as follows

$$\beta_{ji,\min} \leq \beta_{ji}(t) \leq \beta_{ji,\max} \tag{3}$$

where $\beta_{ji,\min}$, $\beta_{ji,\max}$ are the minimum and maximum permissible entrance rate of vehicles, respectively, and $\beta_{ji,\min} > 0$ to avoid long queues and delays at the perimeter of the network and the boundary of neighborhood reservoirs. Moreover, the following constraints are introduced to prevent overflow phenomena within the reservoirs

$$\sum_{i=1}^{N} \Big(\beta_{ji}(t) + \varepsilon_i \Big) \leq 1, \quad \forall\, j = 1, \dots, N,\ j \in \mathcal{S}_i \tag{4}$$

where $\varepsilon_i > 0$ is a portion of uncontrolled flow that enters reservoir i. Finally the accumulation $n_i(t)$ cannot be higher than the maximum accumulation $n_{i,\max}$ for each reservoir i

$$0 \leq n_i(t) \leq n_{i,\max}, \quad \forall\, i = 1, \dots, N. \tag{5}$$

Introducing (2) in (1) we obtain the following nonlinear state equation

$$\frac{dn_i(t)}{dt} = \sum_{j \in \mathcal{S}_i} \beta_{ji}(t) O_j(n_j(t)) - O_i(n_i(t)) + d_i(t). \tag{6}$$

This nonlinear model may be linearized around some set point $\hat{\beta}_{ji}$, $\hat{n}_i$, and $\hat{d}_i$ that satisfy the steady state version of (6). Denoting $\Delta x = x - \hat{x}$ analogously for all variables the linearization yields

$$\begin{aligned} \Delta \dot{n}_i(t) = &\sum_{j \in \mathcal{S}_i} \Delta\beta_{ji}(t) O_j(\hat{n}_j(t)) - \Delta n_i(t) O_i'(\hat{n}_i(t)) + \\ &\sum_{j \in \mathcal{S}_i} \hat{\beta}_{ji}(t) \Delta n_j(t) O_j'(\hat{n}_j(t)) + \Delta d_i(t). \end{aligned} \tag{7}$$

The system in (7) approximates the original system in (6) when we are near the equilibrium point about which the system was linearized. This point should be close to the critical accumulation $\tilde{n}_i$ for each reservoir $i = 1, \dots, N$, where the individual reservoirs' throughput is maximized.

Applying (7) to a network partitioned in N reservoirs the following state equation (in vector form) describes the evolution of the system in time

$$\Delta \dot{\mathbf{n}}(t) = \mathbf{F} \Delta \mathbf{n}(t) + \mathbf{G} \Delta \boldsymbol{\beta}(t) + \mathbf{H} \Delta \mathbf{d}(t) \tag{8}$$

where $\Delta \mathbf{n} \in \mathbb{R}^N$ is the state deviations vector of $\Delta n_i = n_i - \hat{n}_i$ for each reservoir $i = 1, \dots, N$; $\Delta \boldsymbol{\beta} \in \mathbb{R}^M$ is the control deviations vector of $\Delta \beta_{ji} = \beta_{ji} - \hat{\beta}_{ji}$, $\forall\, i = 1, \dots, N$, $j \in \mathcal{S}_i$; $\Delta \mathbf{d} \in \mathbb{R}^N$ is the demand deviations vector of $\Delta d_i = d_i - \hat{d}_i$ for each reservoir $i = 1, \dots, N$; and $\mathbf{F}$, $\mathbf{G}$, and $\mathbf{H}$ are the state, control, and demand matrices, respectively. In particular, $\mathbf{F} \in \mathbb{R}^{N \times N}$ is a square matrix with diagonal elements $F_{ii} = -(1 - \hat{\beta}_{ii}(t)) O_i'(\hat{n}_i(t))$ if $i = j \in \mathcal{S}_i$, and $F_{ii} = -O_i'(\hat{n}_i(t))$ otherwise, and off-diagonal elements $F_{ji} = \hat{\beta}_{ji}(t) O_j'(\hat{n}_j(t))$ if $j \in \mathcal{S}_i$, and

$F_{ji} = 0$ otherwise; $\mathbf{G} \in \mathbb{R}^{N \times M}$ is a rectangular matrix, where $M \leq N^2$ (depends on the network partition and the set $\mathcal{S}_i$, $i = 1, \ldots, N$) with elements $G_{ji} = O_j(\hat{n}_j(t))$ if the origin reservoir j is reachable from the destination reservoir i, and $G_{ji} = 0$ otherwise; $\mathbf{H}$ is an identity square matrix of dimension N. The continuous-time linear state system (8) may be directly translated in discrete-time, using Euler first-order time discretization with sample time T, as follows

$$\Delta\mathbf{n}(k+1) = \mathbf{A}\Delta\mathbf{n}(k) + \mathbf{B}\Delta\boldsymbol{\beta}(k) + \Delta\mathbf{d}(k) \qquad (9)$$

where k is the discrete time index, and $\mathbf{A} = e^{\mathbf{F}T} \approx (\mathbf{I} + \frac{1}{2}\mathbf{A}T)(\mathbf{I} - \frac{1}{2}\mathbf{A}T)^{-1}$, $\mathbf{B} = \mathbf{F}^{-1}(\mathbf{A} - \mathbf{I})\mathbf{G}$ (if $\mathbf{F}$ is nonsingular) are the state and control matrices of the corresponding discrete-time system. This discrete-time linear model (9) will be used as a basis for feedback control design in Section III.

III. Feedback Regulators for Perimeter Control

Multivariable feedback regulators have been applied in the transport area mainly for coordinated ramp metering [15] and traffic signal control [16], [17], [18]. In this work, we present a multivariable feedback regulator derived through the formulation of the problem as an LQ optimal control problem for the design of feedback perimeter control strategies for multi-region and heterogeneously loaded networks.

A. Perimeter Control Objectives

In the case of a single-reservoir system (Fig. 1(a)) which exhibits an MFD, a suitable control objective is to minimize the total time that vehicles spend in the system including both time waiting to enter and time traveling in the network. It is known that the corresponding optimal policy is to allow as many vehicles to enter the network as possible without allowing the accumulation to reach states in the congested regime [12]. However, in the case of a multi-reservoir system (Fig. 1(b)), such a policy may induce uneven distribution of vehicles in the reservoirs, and, as a consequence, may invalidate the homogeneity assumption of traffic loads within the reservoirs and degrade the total network throughput and efficiency. From this, it can be conjectured (and also shown later in the paper) that the critical accumulation $\tilde{n}$ and the maximum throughput $O(\tilde{n})$ of a network modeled as a single-reservoir system are very different from the critical accumulation $\tilde{n}_i$, $i = 1, \ldots, N$ and the maximum throughput $O_i(\tilde{n}_i)$, $i = 1, \ldots, N$ of the same city partitioned in N reservoirs. Moreover, the time each of the reservoirs reaches the congested regime is very different.

A suitable control objective for a multi-reservoir system aims at: (a) distributing the accumulation of vehicles n_i in each reservoir i as homogeneously as possible over time and the network reservoirs, and (b) maintaining the rate of vehicles β_{ji} that are allowed to enter each reservoir around a set (desired) point $\hat{\beta}_{ji}$ while the system's throughput is maximized. A possible way to act in the sense of point (a) is to equalize the distribution of the relative accumulation of vehicles $n_i/n_{i,\max}$ despite inhomogeneous time and space distribution of arrival flows. Requirement (b) is taken by setting the desired point $\hat{\beta}_{ji}$ be equal to the rate of vehicles correspond to output $O_j(\hat{n}_j)$, $i = 1, \ldots, N$, $j \in \mathcal{S}_i$.

B. Multivariable Feedback Regulator

The proposed feedback perimeter and boundary control strategy is based on the multi-reservoir network dynamics (9) and the control objective mentioned in Section III-A. To this end, we consider the following quadratic cost criterion:

$$\mathcal{L}(\boldsymbol{\beta}) = \frac{1}{2}\sum_{k=0}^{\infty}\left(\|\Delta\mathbf{n}(k)\|^2_{\mathbf{Q}} + \|\Delta\boldsymbol{\beta}(k)\|^2_{\mathbf{R}}\right) \qquad (10)$$

where $\mathbf{Q}$ and $\mathbf{R}$ are non-negative definite, diagonal weighting matrices. The first term in (10) is responsible for minimization and balancing of the relative accumulation of vehicles $n_i/n_{i,\max}$ in each reservoir i. To this end, the diagonal elements of $\mathbf{Q}$ are set equal to the inverse of the maximum accumulation of the corresponding reservoirs (see [16], [18] for details). The second term is responsible for objective (b) in Section III-A and the choice of the weighting matrix $\mathbf{R} = r\mathbf{I}$ is performed via a trial-and-error procedure so as to achieve a satisfactory control behavior for a given multi-reservoir network.

Minimization of the performance criterion (10) subject to (9) (assuming $\Delta\mathbf{d}(k) = \mathbf{0}$) leads to the LQ regulator [19]

$$\boldsymbol{\beta}(k) = \hat{\boldsymbol{\beta}} - \mathbf{K}\left[\mathbf{n}(k) - \hat{\mathbf{n}}\right] \qquad (11)$$

where matrix $\mathbf{K}$ is the steady-state solution of the corresponding Riccati equation which depends only upon the problem matrices $\mathbf{A}$, $\mathbf{B}$, $\mathbf{Q}$, and $\mathbf{R}$. Note that the corresponding discrete-time linear system (9) is controllable and reachable and as a consequence a dead-beat gain $\mathbf{K}$ can be off-line calculated for a low value of the scalar weight r.

A potential disadvantage of the LQ theory is that it does not allow for direct consideration of the inequality constraints (3)-(5). In this work, the control constraints (3) are imposed after application of the feedback regulator (11). Regarding the state constraints (5), one may see that the balancing of the relative accumulation of vehicles $(n_i - \hat{n}_i)^2/n_{i,\max}$ via the control objective (10) reduces the risk of a reservoir to reach the congested regime in an indirect way. Finally, the overflow constraints (4) can be satisfied by appropriate selection of $\beta_{ji,\min}$, $\beta_{ji,\max}$.

The regulator (11) is activated in real-time at each sample interval T and only within specific time windows (e.g. by use of two thresholds $n_{i,\text{act}}$ and $n_{i,\text{stop}}$), based on the current accumulation $\mathbf{n}(k)$, to calculate the rates of vehicles $\boldsymbol{\beta}(k)$ to be allowed to enter each reservoir. The required real-time information on the accumulation $\mathbf{n}(k)$ can be directly obtained via mid-block loop detector time-occupancy measurements [16]. After the application of the regulator (11), if the ordered value $\boldsymbol{\beta}(k)$ violates the constraints (3), it should be adjusted to become feasible. The obtained $\beta_{ji}(k)$ values are then converted to arriving flows (by multiplying $\beta_{ji}(k)$ by $O_j(n_j(k))$) and used to define the green periods of the signalized intersections located at the boundary of neighborhood reservoirs or the perimeter of the network. To this end, the latter flows are equally distributed to the corresponding intersections and converted to a (entrance) link green stage duration with respect to the saturation flow of the link and the cycle time of the intersections.

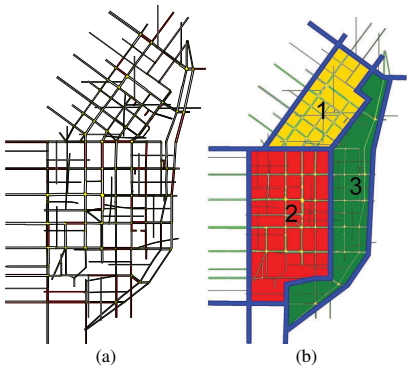

Fig. 2. (a) The test site (b) Partitioning of the network into 3 reservoirs.

IV. Implementation

A. Network Description and Simulation Setup

The test site is a 2.5 square mile area of Downtown San Francisco, including 100 intersections and 400 links. Traffic signals are all multiphase fixed-time operating on a common cycle length of 90 s for the west boundary of the area and 60 s for the rest. The test area is modeled via the AIMSUN microscopic simulator and typical loop-detectors have been installed around the middle of each network link, according to Fig. 2(a). The simulation step for the simulation model of the test site, was set to 0.5 s. For a 4-hours (9:00–12:00) time-dependent scenario with strong demand, ten replications were carried out to account for stochastic effects of the simulator. During this scenario the network is filled and severe congestion is faced for 2 hours with many link queues spilling back into upstream links.

The test site is partitioned into three homogeneous reservoirs ($N = 3$) with small variances of link densities [11], according to Fig. 2(b). The three reservoirs are separated by blue lines in Fig. 2(b), and consist of 112 (yellow colored area), 128 (red colored area), and 147 links (green colored area), respectively. To derive and investigate the shape of the MFDs of the three reservoirs, simulations are performed with a field-applied, fixed-time signal control plan. Based on the derived MFDs the LQ regulator (11) is designed. Then, the perimeter control strategy is applied every $T = 180$ s, a control interval that is twofold or threefold to the cycle length of all the considered intersections. Finally, the perimeter and boundary control resulting from (11) is modified to satisfy the constraints (3). These settings are then forwarded to the 25 signalized intersections located at the boundary of neighborhood reservoirs or the perimeter of the test network for application, i.e. by modifying the green duration of the phases where perimeter and boundary arriving flows are involved.

B. Macroscopic Fundamental Diagrams and Heterogeneity

Fig. 3(a) displays the MFD resulting for the considered demand scenario and ten replications (R1 to R10), each with different seed in AIMSUN. This figure plots the throughput-load relationship (veh vs. veh/h) in the network for the whole simulation time period. Each measurement point in the diagram corresponds to 180 s. As a first remark, Fig. 3(a) confirms the existence of an MFD for Downtown San Francisco with moderate scatter across different replications. It can be seen that the maximun throughput values (around $30 \cdot 10^4$ veh/h) in Fig. 3(a) occur in an accumulation range from 4000 to 6000 vehs. If the accumulation is allowed to increase to values of $n > 6000$ veh, then the network becomes severely congested with states in the congested regime of the MFD, the throughput decreases with accumulation (negative slope) and the system can lead to network-wide gridlock. It is known for a single-reservoir system that in order to prevent this throughput degradation, n should be maintained in the mentioned observed range (close to $\tilde{n} \approx 6000$ veh) during rush while the system's throughput is maximized [12].

Fig. 3(b) displays the MFDs of the three reservoirs resulting for the considered demand scenario and ten replications. It can be seen that all three regions experience MFD with quite moderate scatter across different replications. Nevertheless, there is a clear distinction between congested and uncongested regime for all reservoirs. Note that the time and the accumulation n_i each of the reservoirs reaches the congested regime are very different. The reservoir 3 (red curve) reaches congestion at time 10:30 (for an accumulation $n_3 \approx 1500$ veh) and then it propagates in the reservoirs 2 (green curve) and 1 (blue curve), at time 10:45 (for $n_2 \approx 2000$ veh) and 11:00 (for $n_1 \approx 750$ veh), respectively. This propagation of congestion would not be observable by looking at the unified MFD in Fig. 3(a), which reaches the congestion at time 10:45 for an accumulation $n \approx 6000$ veh. This establishes our conjecture stated in Section III-A. Note as well that the maximun achievable throughput is different for each reservoir $i = 1, 2, 3$ (around $7 \cdot 10^4$ veh/h, $11 \cdot 10^4$ veh/h, and $8 \cdot 10^4$ veh/h, respectively) and occur in accumulation ranges $[500, 1000]$ veh, $[1100, 2250]$ veh, and $[1000, 1700]$ veh, respectively. The difference in maximun flow levels and congested regimes imply corresponding differences of the highest accumulation of vehicles $n_{i,\max}$ that is reached by each reservoir $i = 1, 2, 3$. Thus, reservoir 1 is seen to reach up to 1700 veh, reservoir 2 reaches up to 4250 veh, and reservoir 3 reaches up to 3100 veh. The minimum total flow at maximum load is around $2 \cdot 10^4$ veh/h for all reservoirs.

C. Design of the Feedback Perimeter Controller

The implementation of the proposed perimeter strategy to the test site corresponds to the design and application of the regulator (11). A schematic map of the test site partitioned in $N = 3$ reservoirs is shown in Fig. 2(b). For the proposed partitioning, each reservoir is reachable from the perimeter and the boundary, i.e. $\mathcal{S}_i = \{1, 2, 3\}$, $\forall\, i = 1, 2, 3$. Thus, each reservoir i is equipped with one perimeter controller β_{ii} and two boundary controllers β_{ji}, $j \neq i$. The control vector is given by $\boldsymbol{\beta} = \begin{bmatrix}\beta_{11} & \beta_{21} & \beta_{31} & \beta_{12} & \beta_{22} & \beta_{32} & \beta_{13} & \beta_{23} & \beta_{33}\end{bmatrix}^\tau$. The state vector $\mathbf{n}(k)$ includes the accumulation of vehicles for each reservoir i and is given by $\mathbf{n} = \begin{bmatrix}n_1 & n_2 & n_3\end{bmatrix}^\tau$. The set point $\hat{n}_i$ for each reservoir i is selected within the optimal range of the corresponding MFD for maximum throughput, given the analysis in the previous section. More specifically, the following values $\hat{n}_1 = 600$ veh,

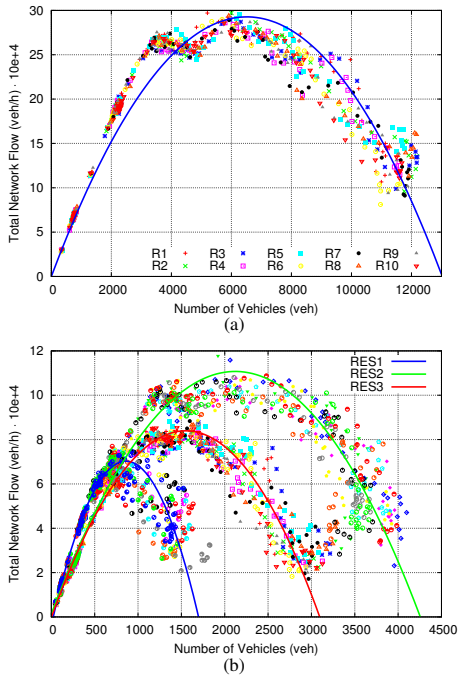

Fig. 3. Macroscopic Fundamental Diagrams (a) of the whole network and (b) of the three reservoirs.

TABLE I

PIs OF THE PERIMETER CONTROL STRATEGY VS. NO CONTROL.

Evaluation Criteria	NO CONTROL	PERIMETER CONTROL	IMPROVEMENT (%)	Units
Virtual Queue (t_end)	13757	14935	8,6	*veh*
N Total (t_end)	11702	8773	-25,0	*veh*
TTS without VQ	18460	16296	-11,7	*veh-hrs*
TTS with VQ	21317	20105	-5,7	*veh-hrs*
Speed without VQ	5,82	6,71	15,4	*km/hr*
Speed with VQ	5,04	5,44	8,0	*km/hr*
Total output	55076	56057	1,8	*vehs*
TDT	107404	109375	1,8	*km*

$\hat{n}_2 = 1250$ veh, and $\hat{n}_3 = 1100$ veh are selected for the current implementation (see Fig. 3(b)). The desired rate of the control inputs are based on the corresponding $O_i(\hat{n}_i)$ values for each reservoir i and given by $\hat{\boldsymbol{\beta}} = \begin{bmatrix}0.3 & 0.2 & 0.25 & 0.35 & 0.25 & 0.35 & 0.3 & 0.2 & 0.25\end{bmatrix}^\tau$. Finally, the minimum and maximum permissible rates are given by $\boldsymbol{\beta}_{\min} = \mathbf{0.1}^\tau$ and $\boldsymbol{\beta}_{\max} = \begin{bmatrix}0.6 & 0.4 & 0.5 & 0.7 & 0.5 & 0.7 & 0.6 & 0.4 & 0.5\end{bmatrix}^\tau$, respectively.

For the derivation of the gain matrix $\mathbf{K} \in \mathbb{R}^{9\times 3}$ in (11) it suffices to specify the state matrices $\mathbf{A} \in \mathbb{R}^{3\times 3}$, $\mathbf{B} \in \mathbb{R}^{3\times 9}$, and the weighting matrices $\mathbf{Q} \in \mathbb{R}^{3\times 3}$, $\mathbf{R} \in \mathbb{R}^{9\times 9}$. The state matrices are developed for the particular network on the basis of the selected set (desired) point $\hat{\mathbf{n}}, \hat{\boldsymbol{\beta}}$ and the linearization according to (7) and (9). The weighting matrices $\mathbf{Q}$, $\mathbf{R}$ in the quadratic cost criterion (10) are chosen diagonal. More precisely, the diagonal elements of $\mathbf{Q}$ are set equal to the inverse of the maximum accumulation of the corresponding reservoirs, i.e. $Q_{ii} = 1/n_{i,\max}$, $i = 1, 2, 3$ (see Sections III-A, III-B). Finally, the diagonal elements of matrix $\mathbf{R}$ were set equal to $r = 0.00001$. This low value of the scalar weight r was found to lead to a dead-beat gain $\mathbf{K}$ (not shown).

D. Results

Table I displays the obtained results in terms of the indices *Total Time Spent* (TTS), *Total Distance Traveled* (TDT), *Space-mean Speed*, and *total number of vehicles that exit the network* (Total output) during the whole scenario for the Perimeter Control (PC) and No Control (NC) cases. This table also displays the virtual waiting queues (in veh) that have been stored at the origin links of the network and the number of vehicles within network links inside the three reservoirs at the end of simulation, Virtual Queue (t_end) (VQ) and N total (t_end), respectively, because the network is not empty at the end of the simulation. Thus, speed and TTS were also calculated taking into account the VQ. Note that by directly extracting performance measures of speed or TTS from the simulator will not include vehicles waiting outside the network (virtual queues), which will consistently underestimate the time spent of gated/controlled vehicles.

As can be seen in Table I, the PC strategy leads to an improvement of the evaluation criteria compared to NC for the whole network. When PC is applied, TTS and speed are improved in average by 11.7% (5.7% with VQ) and 15.4% (8% with VQ), respectively, compared to NC. In contrast, the higher virtual waiting queue in PC (8.6% compared to NC) indicates that the control action creates temporary queues at the perimeter of the network (β_{ii} controllers). However, this proves propitious for the total network throughput and the traffic state inside the three reservoirs as we will see later. Finally, the lower number of vehicles within the network links (N Total) at the end of simulation (25% compared to NC) indicates that the control action does not create queues that spill back to upstream intersections at the boundary of neighborhood reservoirs (β_{ji}, $i \neq j$, controllers). The simulation ends with a high demand and congestion in the network. In case a decreasing demand was applied after the end of the simulation to reach non-congested states, the benefits are expected to be much higher.

Figs 4(a), 4(b) display the MFDs of the three reservoirs resulting for the demand scenario and one replication when NC and PC are applied, respectively. Clearly, when PC is applied, the three reservoirs remain semi-congested and only a few states observed in the congested regime; under NC, the network becomes severely congested with states in the congested regime of the corresponding MFDs. Note that, in absence of perimeter control, the throughput at the end of the simulation is around $2 \cdot 10^4$ veh/h for all reservoirs.

The accumulation and flow of the three reservoirs for one replication are depicted in Figs 4(c), 4(d) and Figs 4(e), 4(f), respectively. Traffic conditions are identical for both control cases up to around 09:15, when PC is switched on (due to reservoir 3), as accumulation n_i reaches its set point $\hat{n}_i$ for each reservoir i, albeit at different times, the perimeter strategy (a) limits the rate at which arriving vehicles are allowed to enter the network to keep it from becoming congested, and (b) manages the intertransfers between the reservoirs to respect homogeneity in loads and the network reservoirs over time. Thus, throughput is maintained at high levels within the three reservoirs that is close to the target points $O(\hat{n}_i)$ for each reservoir i (corresponding to $\hat{\boldsymbol{\beta}}$), i.e. around $6 \cdot 10^4$ veh/h, $8.5 \cdot 10^4$ veh/h, and $7 \cdot 10^4$ veh/h (see Fig. 4(d)), respectively, in contrast to the NC case (see Fig. 4(b)). Remarkably, the accumulation n_i of each reservoirs i is not exactly maintained to $\hat{n}_i$ (see Fig. 4(b)) thanks to

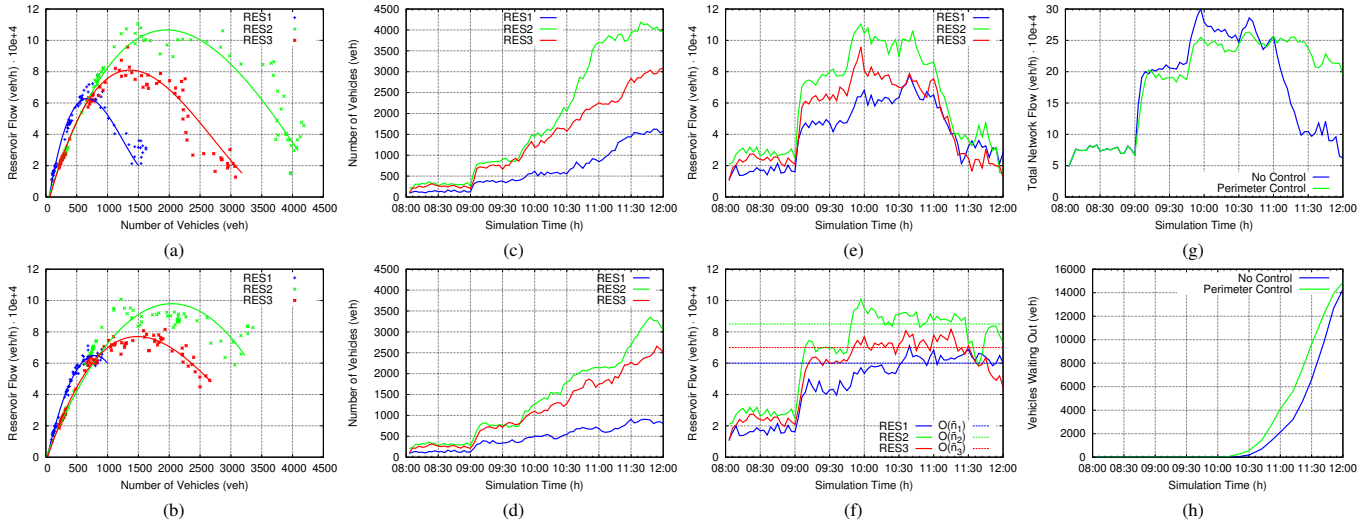

Fig. 4. MFDs of the three reservoirs for one replication (a) with NC, (b) with PC; Reservoir accumulation of vehicles over time (c) with NC, (d) with PC; Reservoir flow over time (e) with NC, (f) with PC; (g) Total network flow over time; (h) Vehicles waiting out of the network over time.

the selection of the weights $Q_{ii} = 1/n_{i,max}$ in the control objective (10). Fig. 4(g), 4(h) show the throughput (total flow of all links in the network) and the virtual waiting queues for the same replication, respectively. Fig. 4(g) indicates that the perimeter strategy maintains the overall throughput to high values (via appropriate actions within the reservoirs) during the heart of the rush (after 10:30), compared to the NC case, even if it involves longer waiting queues at the origins of the network (cf. Fig. 4(h), Table I)). This underlines that appropriate designed perimeter control strategies for multi-reservoir systems might prove beneficial in ameliorating deficiencies associated with single-reservoir systems (e.g. propagation of congestion).

V. Conclusions

In this paper, we addressed the problem of perimeter control for congested multi-reservoir networks. To the best of our knowledge, this is the first approach towards the development of generic, elegant, and efficient perimeter control strategies that appropriately account for the spatial and temporal heterogeneity of congestion between the reservoirs. Future work will deal with the comparison of the feedback perimeter control strategy with other approaches in simulation, and its application in real-life conditions. Adaptive fine-tuning of the design gain in (11) should also be a research priority [20].

References

[1] B. Greenshields, "A study in highway capacity," in *Proc. Highway Res Board*, vol. 14, 1935, pp. 448–477.

[2] B. S. Kerner and H. Rehborn, "Experimental properties of complexity in traffic flow," *Phys Rev*, vol. 53E, pp. R4275–R4278, 1996.

[3] L. Leclercq, J. Laval, and N. Chiabaut, "Capacity drops at merges: an endogenous model," *Transport Res*, vol. 45B, no. 9, pp. 1302–1313, 2011.

[4] N. Geroliminis and C. F. Daganzo, "Existence of urban-scale macroscopic fundamental diagrams: Some experimental findings," *Transport Res*, vol. 42B, no. 9, pp. 759–770, 2008.

[5] C. Buisson and C. Ladier, "Exploring the impact of homogeneity of traffic measurements on the existence of macroscopic fundamental diagrams," *Transport Res Rec*, vol. 2124, pp. 127–136, 2009.

[6] Y. Ji, W. Daamen, S. Hoogendoorn, S. Hoogendoorn-Lanser, and X. Qian, "Macroscopic Fundamental Diagram: Investigating its shape using simulation data," *Transport Res Rec*, vol. 2161, pp. 42–48, 2010.

[7] A. Mazloumian, N. Geroliminis, and D. Helbing, "The spatial variability of vehicle densities as determinant of urban network capacity," *Philos Trans Royal Soc*, vol. 368A, no. 1928, pp. 4627–4647, 2010.

[8] C. Daganzo, V. Gayah, and E. Gonzales, "Macroscopic relations of urban traffic variables: Bifurcations, multivaluedness and instability," *Transport Res*, vol. 45B, no. 1, pp. 278–288, 2011.

[9] K. Aboudolas, M. Papageorgiou, A. Kouvelas, and E. Kosmatopoulos, "A rolling-horizon quadratic-programming approach to the signal control problem in large-scale congested urban road networks," *Transport Res*, vol. 18C, no. 5, pp. 680–694, 2010.

[10] N. Geroliminis and J. Sun, "Hysteresis phenomena of a macroscopic fundamental diagram in freeway networks," *Transport Res*, vol. 45A, pp. 966–979, 2011.

[11] Y. Ji and N. Geroliminis, "On the spatial partitioning of urban transportation networks," *Transport Res*, vol. 46B, no. 10, pp. 1639–1656, 2012.

[12] C. F. Daganzo, "Urban gridlock: Macroscopic modeling and mitigation approaches," *Transport Res*, vol. 41B, no. 1, pp. 49–62, 2007.

[13] M. Keyvan-Ekbatani, A. Kouvelas, I. Papamichail, and M. Papageorgiou, "Exploiting the fundamental diagram of urban networks for feedback-based gating," *Transport Res*, vol. 46B, no. 10, pp. 1393–1403, 2012.

[14] N. Geroliminis, J. Haddad, and M. Ramezani, "Optimal perimeter control for two urban regions with macroscopic fundamental diagrams: A model predictive approach," *IEEE Trans Intell Transp Sys*, vol. 14, no. 1, pp. 348–359, 2013.

[15] M. Papageorgiou, J. Blosseville, and H. Hadj-Salem, "Modelling and real-time control of traffic flow on the southern part of Boulevard Périphérique in Paris Part II: Coordinated on-ramp metering," *Transport Res*, vol. 24A, no. 5, pp. 361–370, 1990.

[16] C. Diakaki, M. Papageorgiou, and K. Aboudolas, "A multivariable regulator approach to traffic-responsive network-wide signal control," *Control Eng Pract*, vol. 10, pp. 183–195, 2002.

[17] C. Diakaki, V. Dinopoulou, K. Aboudolas, M. Papageorgiou, E. Ben-Shabat, E. Seider, and A. Leibov, "Extensions and new applications of the traffic-responsive urban control strategy: Coordinated signal control for urban networks," *Transport Res Rec*, no. 1856, pp. 202–211, 2003.

[18] K. Aboudolas, M. Papageorgiou, and E. B. Kosmatopoulos, "Store-and-forward based methods for the signal control problem in large-scale congested urban road networks," *Transport Res*, vol. 17C, no. 2, pp. 163–174, 2009.

[19] M. Papageorgiou, *Optimierung*, 2nd ed. Munich, Germany: Oldenbourg, 1996.

[20] A. Kouvelas, K. Aboudolas, E. Kosmatopoulos, and M. Papageorgiou, "Adaptive performance optimization for large-scale traffic control systems," *IEEE Trans Intell Transp Sys*, vol. 12, no. 4, pp. 1434–1445, 2011.